Received: 5 October 2022 | Revised: 17 November 2022 | Accepted: 12 December 2022

DOI: 10.1002/pro.4543

FULL-LENGTH PAPER

THE PROTEIN SOCIETY WILEY

Hyperthermostable recombinant human heteropolymer ferritin derived from a novel plasmid design

Ayush K. Srivastava[1] | **Lucas J. Scalcione**[1] | **Paolo Arosio**[2] | **Fadi Bou-Abdallah**[1]

[1]Department of Chemistry, State University of New York, Potsdam, New York, USA

[2]Department of Molecular & Translational Medicine, University of Brescia, Brescia, Italy

Correspondence
Fadi Bou-Abdallah, Department of Chemistry, State University of New York, Potsdam, NY 13676, USA.
Email: bouabdf@potsdam.edu

Funding information
National Institute of Health, Grant/Award Number: R15GM104879; National Science Foundation, Grant/Award Numbers: 0921364, 1934666; Research Corporation for Science Advancement, Grant/Award Number: 27452

Review Editor: Jeanine Amacher

Abstract

Mammalian ferritins are predominantly heteropolymeric species consisting of 2 structurally similar, but functionally and genetically distinct subunit types, called H (Heavy) and L (Light). The two subunits co-assemble in different H and L ratios to form 24-mer shell-like protein nanocages where thousands of iron atoms can be mineralized inside a hollow cavity. Here, we use differential scanning calorimetry (DSC) to study ferritin stability and understand how various combinations of H and L subunits confer aspects of protein structure–function relationships. Using a recently engineered plasmid design that enables the synthesis of complex ferritin nanostructures with specific H to L subunit ratios, we show that homopolymer L and heteropolymer L-rich ferritins have a remarkable hyperthermostability (Tm = 115 ± 1°C) compared to their H-ferritin homologues (Tm = 93 ± 1°C). Our data reveal a significant linear correlation between protein thermal stability and the number of L subunits present on the ferritin shell. A strong and unexpected iron-induced protein thermal destabilization effect (ΔT_m up to 20°C) is observed. To our knowledge, this is the first report of recombinant human homo- and hetero-polymer ferritins that exhibit surprisingly high dissociation temperatures, the highest among all known ferritin species, including many known hyperthermophilic proteins and enzymes. This extreme thermostability of our L and L-rich ferritins may have great potential for biotechnological applications.

KEYWORDS

differential scanning calorimetry (DSC), human ferritin, hyperthermostability, iron core, iron homeostasis

1 | INTRODUCTION

The ubiquitous and well-characterized iron storage protein, ferritin, is a highly conserved supramolecular nanostructure that plays a key role in iron homeostasis (Arosio et al., 2009; Bou-Abdallah, 2010; Chasteen & Harrison, 1999; Harrison & Arosio, 1996; Mehlenbacher et al., 2017; Theil, 2013; Theil et al., 2016). Mammalian ferritins are typically composed of 2 subunit types, referred to as H (~21,000 Da) and L (~19,000 Da). The two subunits co-assemble in various proportions with tissue-specific distribution (isoferritins) to form a 24-subunit shell-like protein nanocage (of ~8 nm inner cavity and ~12 nm outer diameter), within which thousands of iron atoms can be stored in the form of insoluble inorganic ferrihydrite core. Whereas the H-subunits rapidly oxidize redox-active ferrous ions at their diiron ferroxidase centers, the L-subunits lack such centers but provide efficient iron nucleation sites that facilitate the formation of the iron mineral core through a high density

of acidic residues (i.e. carboxyl groups) present on the protein's inner cavity (Bou-Abdallah, 2010; Chasteen & Harrison, 1999; Harrison & Arosio, 1996; Levi et al., 1994; Lopez-Castro et al., 2012; Pozzi et al., 2017; Santambrogio et al., 1993). L-rich ferritins function as long-term iron storage and predominate in iron storage organs such as the liver and the spleen, whereas H-rich ferritins predominate in organs with low iron content such as the heart and the brain (Harrison & Arosio, 1996).

Although the H- and L-subunits are encoded by two distinct genes located on chromosome 11 (for the H-chain) and chromosome 19 (for the L-chain), the co-assembly of the two subunits occur both in vivo (Cozzi et al., 2000), and in vitro (Carmona et al., 2017). A recent study (Srivastava et al., 2021) by our group using an engineered plasmid revealed an original system that can be easily tuned by altering the concentrations of two inducers (isopropyl β-D-1-thiogalactopyranoside, IPTG, and anhydrotetracycline, Tet), allowing the synthesis of a full spectrum of heteropolymer ferritins, from homopolymer L-ferritin (H_0:L_{24}), to homopolymer H-ferritin (H_{24}:L_0), to any combinations of H and L subunits in between, generating a variety of L-rich and H-rich ferritins. Briefly, using a commercially available vector from Addgene, we engineered our own ferritin plasmid in which the cDNA of human ferritin H-subunit (FtH) is cloned downstream the T7 promoter (controlled by Lac I repressor and induced by IPTG) and the cDNA of human ferritin L-subunit (FTL) downstream the Tet-On system (controlled by tetO operator and induced by anhydrotetracycline, Tet). This original design (Srivastava et al., 2021) can be easily tuned by altering the concentrations of the two inducers allowing the synthesis of a full spectrum of heteropolymer ferritins, from H-rich to L-rich ferritins and any combinations in-between. Although the subunits' assembly mechanism remains unknown, an in vitro resonance energy transfer (FRET) investigation (Carmona et al., 2017) demonstrated the preferential formation of H/L hybrid heteropolymers over either H–H or L–L homodimers (Pozzi et al., 2017). However, it is unclear whether a similar mechanism occurs in vivo and what factors or cellular conditions might affect such assembly. Furthermore, although vertebrate ferritins are composed of a mixture of H- and L-subunits, structural information on H/L heteropolymer ferritins do not exist, and crystallographic x-ray structures have only been determined for recombinant homopolymer ferritins composed of a single subunit type (i.e. amphibian H or L, human H, horse L, and mouse L) (Crichton & Declercq, 2010). The first and only resolved x-ray structure of a secreted heteropolymer ferritin is from the cabbage looper/tiger moth *Trichoplusia ni*, formed of H-L chain dimers that are arranged with tetrahedral (T or 23) symmetry (Hamburger et al., 2005), unlike bacterial or vertebrate ferritins, both of which have octahedral (O or 432) symmetry structures.

From a structural viewpoint, extensive inter- and intra-subunits interactions (i.e., hydrophobic, electrostatic, hydrogen bonds, and salt bridges) confer to the ferritin molecule an unusually high thermal and chemical stability. It is the intermolecular main-chain/side-chain and side-chain/side-chain hydrogen bonds and salt bridges that contribute most to the stability of the 24-mer protein. The greater stability of L-subunits is due to the presence of a specific salt bridge (between Lys62 and Glu107) that does not exist on H-subunits; the corresponding residues on the H-subunit (i.e. Glu62 and Glu107) are part of the diiron ferroxidase site (Crichton & Declercq, 2010; Lawson et al., 1989; Santambrogio et al., 1992). In support of this much larger stability conferred by L-subunits, the L-rich horse spleen ferritin (> 90% L) is shown to denature at a much higher temperature than homopolymer H-ferritin (i.e. ~93 vs. 77°C) at pH 7.0 (Simonetta Stefanini et al., 1996). Substitution of L-homopolymers inter-subunit residues along three- and four-fold axes by corresponding H-homopolymer residues resulted in lower protein stability (Levi et al., 1993; Santambrogio et al., 1992; Santambrogio et al., 1997). Other types of amino acid substitutions induced by the introduction of frameshift mutations on L-subunits had a strong destabilization effect on the protein structural integrity, the severity of which depended on the location of the frame shift mutation (McNally et al., 2019). Altogether, these results demonstrate an important role of L-subunits toward ferritin's overall stability.

To our knowledge, there are no direct thermostability measurements of *E. coli* expressed human heteropolymer ferritins, nor has a stability comparison of different heteropolymer ferritins having different H to L subunit ratios been performed. Here, for the first time, our study offers important structural insights into how various combinations of H and L subunits confer extreme thermal stability to the protein, the highest among many ferritin species and hyperthermophilic proteins. Our data may have uncovered significant physiological implications of in vivo iron management, in that a less stable iron-laden ferritin could facilitate ferritin sensing and degradation followed by iron retrieval and recycling. Moreover, a highly stable heteropolymer ferritin may offer important biotechnological applications ranging from a robust bio-nano-template for the synthesis of bio-nano- materials, to the encapsulation and delivery of bioactive compounds or drugs, and industrial food science applications, particularly those requiring thermal processing (Zhang et al., 2020).

Using an original expression system and a novel plasmid design that was developed in our lab (Srivastava et al., 2021), this study was undertaken to measure the unfolding and denaturation thermograms of several human H-rich and L-rich heteropolymers and compare them to the H- and L-ferritin homopolymers, using

differential scanning calorimetry (DSC). Our results reveal hyperthermostability profiles for 100% L-ferritin and L-rich ferritins (H_2:L_{22} and H_6:L_{18}) reaching a melting point (Tm) as high as 115°C. Much lower stability profiles are observed for H- and H-rich ferritins with Tm values in the 90–95°C range. This remarkable thermostability of L- and L-rich ferritins has never been reported before and suggests that a highly robust ferritin nanocage structure is obtained using our engineered plasmid with potentially important biotechnological applications.

2 | RESULTS

2.1 | Ferritin assembly and subunit composition

To examine the protein integrity and the H to L subunit composition of ferritin, SDS and native-PAGE experiments were performed on several homopolymer and heteropolymer ferritin samples. The 7% native-PAGE in Figure 1 shows single bands for heteropolymer ferritin samples, the mobility of which depended on their H to L subunit composition (i.e., H-rich ferritins were close to the homopolymer H-ferritin, whereas L-rich ferritins were closer to the homopolymer L-ferritin, and the ~50/50 H/L somewhere in between). The two sharp bands observed on 12% SDS-PAGE, with similar migration to the individual H and L subunits, suggest that the single bands observed on native PAGE represent one type of ferritin species (i.e., a 24-mer heteropolymer ferritin that has assembled from individual H and L subunits). A preliminary semi-quantitative analysis of SDS-PAGE band intensity was performed on a Kodak 1D image analysis software (v. 3.6.3) or the NIH ImageJ software (Srivastava et al., 2021), and revealed a ferritin subunit composition within 5% of that predicted experimentally by capillary gel electrophoresis (CGE) under denaturing conditions (more below).

2.2 | Capillary gel electrophoresis (SDS-CGE)

To accurately quantify the ferritin heteropolymer subunit composition, SDS-CGE experiments were conducted under denaturing conditions. The SDS-CGE electropherograms

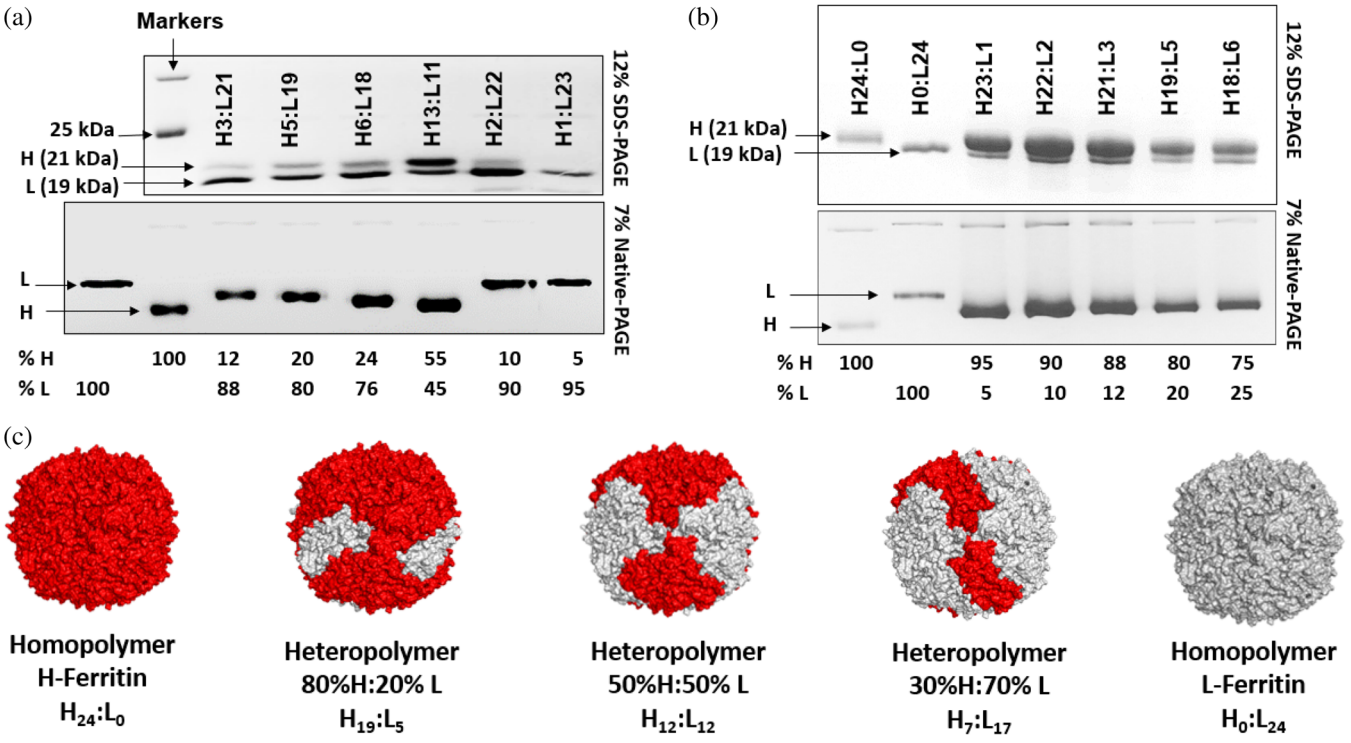

FIGURE 1 (a,b) Coomassie blue stained native-PAGE (7.5%) and SDS–PAGE (12%) of homopolymer H-ferritin (H_{24}:L_0) and L-ferritin (H_0:L_{24}) (0.5–1 μg), and of different heteropolymer ferritin samples as noted on the gels. The ferritin subunits are denoted H (21 kDa) and L (19 kDa) and their relative positions are marked on the left hand side of each gel. The heteropolymer ferritin samples and their H and L percent composition are indicated on each gel next to their corresponding band(s). All protein preparations were performed in LB media from Teknova and the gels were repeated at least 3 times. Note that the different band intensities on native PAGE are due to different purification yield and different protein concentrations injected in each well. (c) Arbitrary computer generated models of human ferritins (homopolymers and heteropolymers) depicting an H_{24}:L_0 (homopolymer H-ferritin), H_{19}:L_5, H_{12}:L_{12}, and H_7:L_{17} heteropolymers, and an H_0:L_{24} (homopolymer L-ferritin). The ferritin models are generated using PyMOL molecular graphics system, v. 2.5.4, Schrödinger, LLC, and the distribution of the H-subunits (red) and L-subunits (gray) is randomly depicted since the structures of human heteropolymer ferritins are unknown.

of homopolymer and heteropolymer ferritins are displayed in Figure 2 and show well-resolved peaks for the L- and H-subunits, separated by about 30 s. From the area under the CE peaks, the subunit composition of the various heteropolymer ferritins were calculated and are shown next to each electropherogram and on the gels of Figure 1.

2.3 | Ferritin thermal stability measured by differential scanning calorimetry (DSC)

To examine the thermal stability of ferritin, differential scanning calorimetry (DSC) experiments were performed between 25 and 125°C, using human homopolymer and heteropolymer ferritins with different H to L subunit ratios (Figure 3). For easy viewing and comparison, the DSC profiles of all ferritin samples employed in this study are displayed as a plot of relative heat capacity versus temperature (Figure 3a). A plot of the Tm values as a function of the number of L-subunits displayed a linear relationship, suggesting a strong effect of L-subunits on the overall thermal stability of the protein (e.g., the more L-subunits present in the ferritin shell structure, the higher the protein stability).

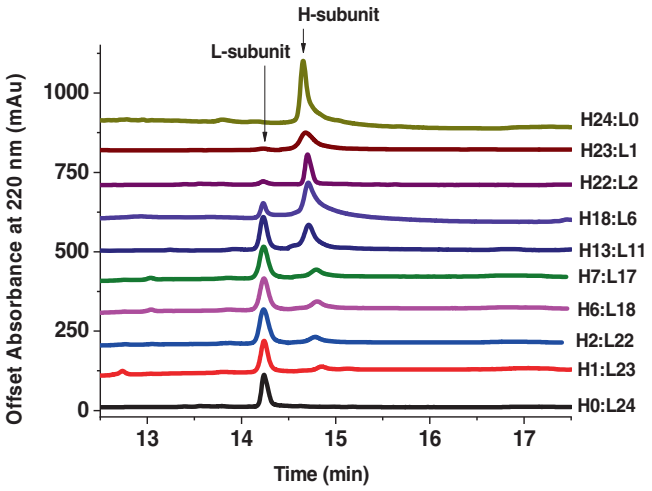

FIGURE 2 Representative SDS-CGE electropherograms of recombinant human ferritin H- and L-homopolymers (also denoted as H_{24}:L_0 and H_0:L_{24}, respectively), and different H/L heteropolymer ferritin samples (all apo-ferritins). Typical protein concentrations ranged between 1 to 2 mg/mL. The instrument conditions are specified under materials and methods. Note that the absorbance values on the Y-axis are arbitrary and have been shifted upward for each of the traces shown above the original black thermogram for easy viewing and comparison. Each electropherogram was repeated at least 2 or 3 times.

2.4 | Effect of iron loading on ferritin thermal stability

To examine the effect of iron loading on the protein thermal stability, several ferritin samples (H- and L-homopolymers, and H-rich and L-rich heteropolymers) were exogenously loaded with 500 Fe(III)/shell each, added in increments of 100 Fe(II)/shell per injection, with adequate time between injections to allow full Fe(II) oxidation (Mehlenbacher et al., 2017; Srivastava et al., 2021) (see Materials and Methods for more details).

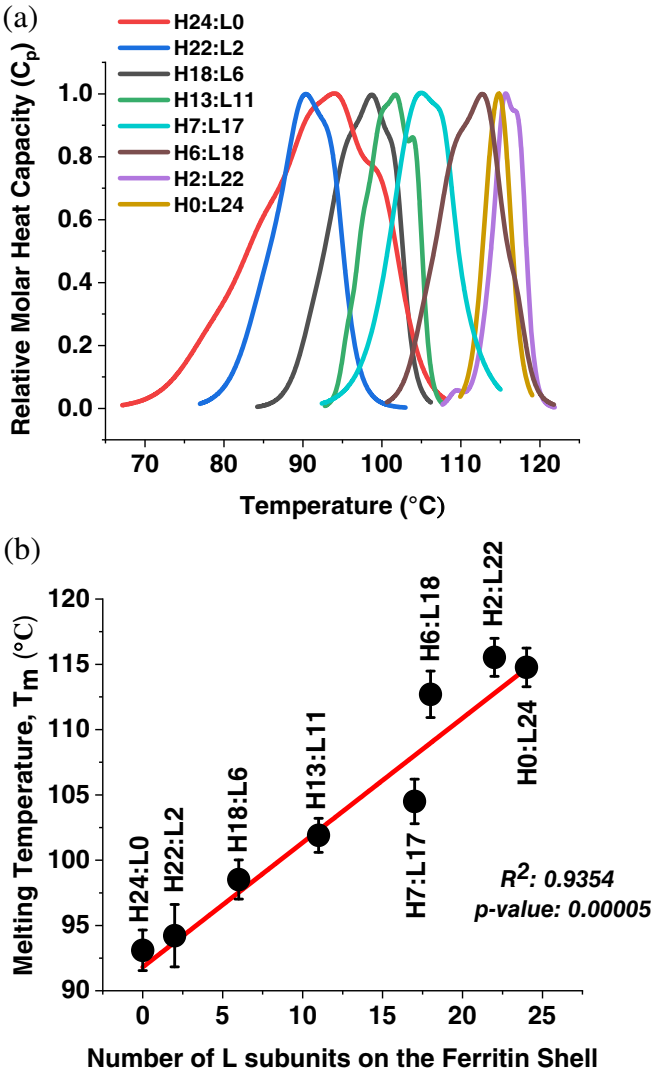

FIGURE 3 (a) Representative baseline-adjusted DSC endotherms plotted as relative heat capacity versus temperature (for easy viewing and comparison) of different apo-ferritin samples. (b) Plot of the melting temperature as a function of the number of L-subunits on the ferritin molecule. Conditions: Apo-ferritin samples (0.5 ± 0.1 mg/mL) are prepared in 50 mM phosphate buffer, 50 mM NaCl, pH 7.4. The experimental pressure was 3.00 atm ± 0.03 atm. The error bars represent a standard deviation from multiple runs, at least 2 runs per sample.

We note that because our *E. coli* expressed and purified ferritin samples contained on average ~ 200 Fe(III)/shell, the total amount of iron present in these samples is therefore ~700 Fe(III)/shell. Figure 4a shows an overlay of the DSC thermograms for both iron-loaded (solid lines) and *E. coli* purified ferritin (dotted lines). Clearly, all the exogenously iron-loaded ferritin samples exhibited a lower thermal stability compared to their apo counterparts (Figure 4b), suggesting that the inner iron core has weakened the structure of the 24-mer assembly and altered the subunit-subunit inter- and intra-molecular interactions (more below).

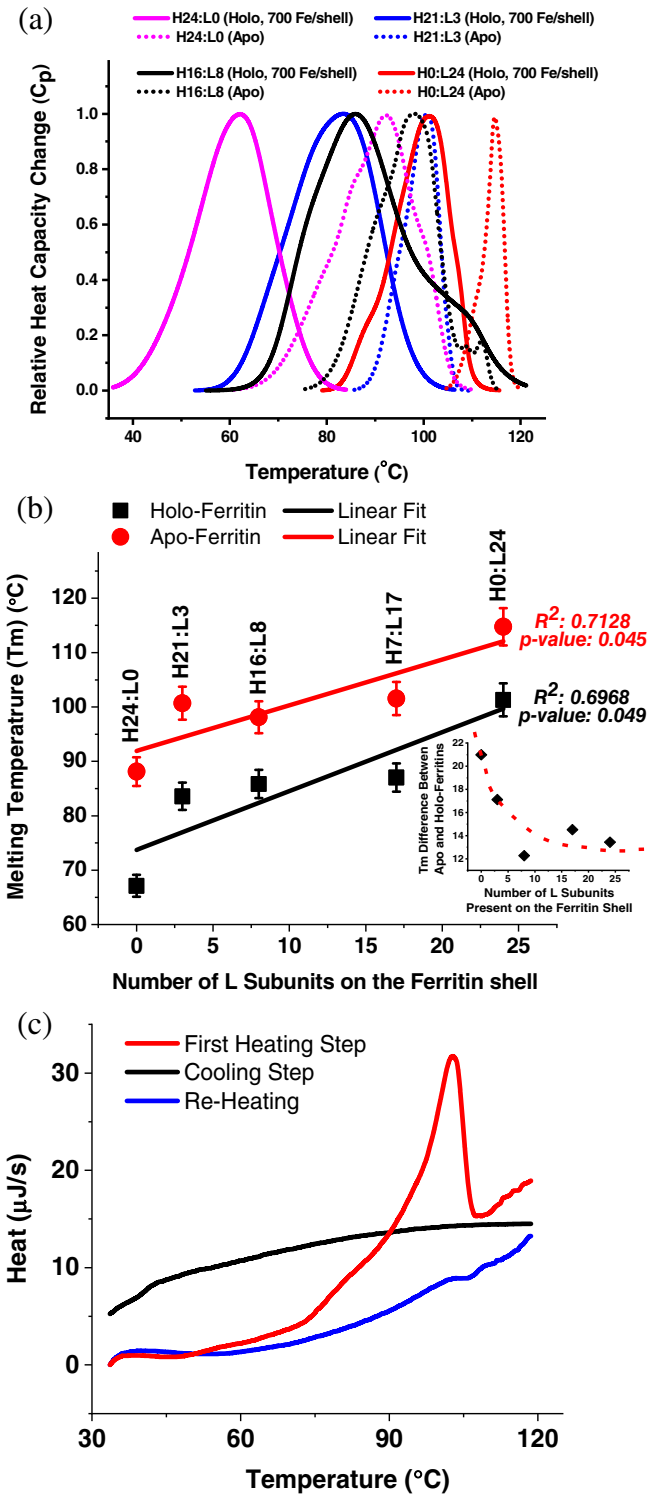

2.4.1 | CD spectra and melting curves

To test whether structural changes occur during iron loading into ferritin and to confirm the stability difference between iron-free and iron-loaded ferritin, we performed circular dichroism (CD) experiments (Figure 5) using an apo-ferritin sample and a holo-ferritin sample loaded with ~1000 Fe(III)/shell. The CD results revealed a lower helical content of the holo-protein compared to the apo-protein (Figure 5a), suggesting that some structural changes have occurred following iron loading. The CD changes manifested in lower thermal stability and partial unfolding of the iron-loaded ferritin, corroborated by the irreversible denaturation of the holo-protein and its inability to refold properly compared to the apo-protein, after T melt (Figure 5a). Although we are unable to quantify Tm from CD melting curves (due to the smaller range of temperature achieved by CD compared to DSC), the result is nonetheless consistent with our DSC data and show that the H-rich heteropolymer holo-ferritin (i.e., H_{19}:L_5) starts to unfold at about 10°C lower than the apo-ferritin (Figure 5b).

2.4.2 | Nature of the inter- and intra-subunits interactions

To explore the nature of the extensive inter- and intra-subunits interactions with the ferritin 24-mer assembly, and provide some insights from a structural viewpoint on

FIGURE 4 (a) Representative DSC thermograms (relative heat capacity vs. temperature) of iron-loaded (holo) and apo-ferritin samples. (b) Plot of the melting temperature as a function of the number of L-subunits present on the ferritin shell, for both exogenously iron-loaded (Holo, total of ~700 Fe/shell) and apo (as expressed in *E. coli* and purified) ferritin samples. (Inset b) difference in Tm values between apo- and holo-ferritins as a function of the number of L-subunits present on the ferritin shell. (c) DSC thermograms of an H-rich apo-ferritin (H_{21}:L_3) following a 3-step cycle: Heating, cooling, and re-heating. Conditions: Ferritin samples (0.5 ± 0.1 mg/mL) are prepared in 50 mM phosphate buffer, 50 mM NaCl, pH 7.4. The experimental pressure was 3.00 atm ± 0.03 atm. The error bars represent a standard deviation from multiple runs, at least 2 runs per sample.

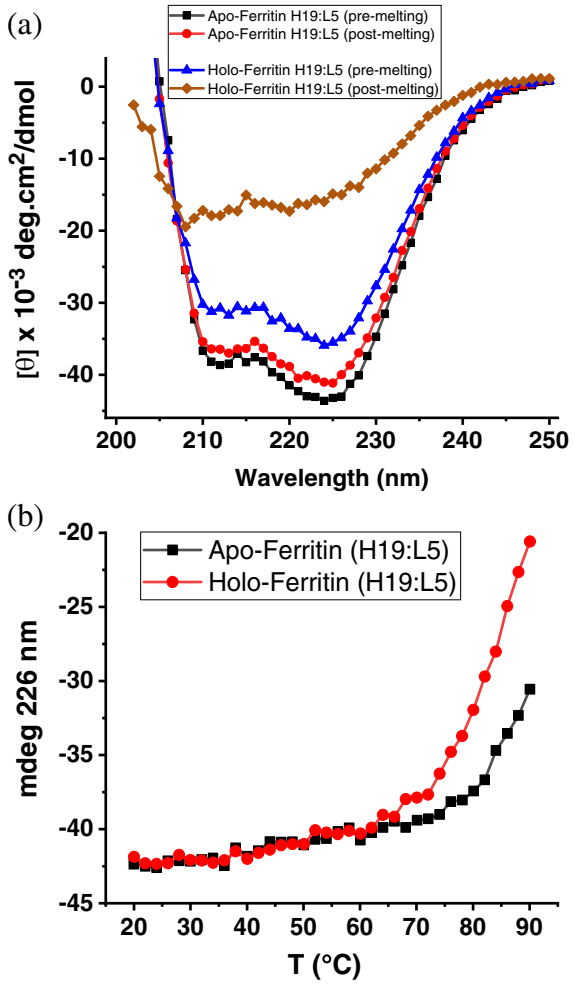

FIGURE 5 (a) Overlay of far UV CD spectra of apo and holo-ferritin samples (H_{19}:L_5) pre- and post-melting collected at 20°C showing the helical content of ferritin. While very similar pre- and post-melting spectra were recorded for apo-ferritin, presumably because H_{19}:L_5 unfolds at >98°C and the highest CD temperature used was 90°C, holo-ferritin (~1000 Fe(III)/shell) revealed lower helical content pre-melting and a significant/complete loss of helical content after melting, suggesting irreversible denaturation and inability to refold, in accord with our DSC results. (b) CD melting temperature curves of the apo- and holo-ferritin samples (H_{19}:L_5). Conditions: 0.2 mg/mL proteins prepared in water, pH 7.4.

the hyperthermal stability of recombinant human ferritins, the total number of hydrogen bonds was calculated with HBPLUS (McDonald & Thornton, 1994) and divided into three main classes; class I is the number of H-bonds formed between main-chain atoms only (MM), class II is the number of H-bonds between main-chain and side-chain atoms (MS/SM), and class III is the number of H-bonds between side-chain atoms only (SS). The HBPLUS software determines the salt bridges and includes them as a subset of the SS hydrogen bonds. The MM bonds are mostly intramolecular (i.e., within the same monomer or subunit) interactions that provide stability of the ferritin secondary structure (α-helices), whereas the MS/SM and SS intramolecular H-bonds confer stability to the 3D fold of the individual subunits. As to the intermolecular (i.e., between neighboring monomers or subunits) MS/SM and SS hydrogen bonds, they are critical for the stability of the 24-mer ferritin assembly. Table 1 shows a comparison of the total number of H-bonds, including salt bridges, in a number of ferritins from different sources, as calculated by HBPLUS. The MS/SM and SS hydrogen bonds do not appear to play an important role in the thermostability of the protein since *P. furiosus* has the lowest numbers of these types of bonds but is one of the ferritins with the highest thermostability. However, an interesting trend emerges from the dominant MM class of bonds where the number of MM hydrogen bonds appear to correlate with the melting temperature, suggesting that the additional 300–400 H-bonds present in the top two hyperthermostable ferritins (human L-ferritin and *P. furiosus*) confer an extra thermostability to these proteins (Table 1, Figure 6).

2.4.3 | Effect of a small endogenous iron core

To investigate whether the presence of the small iron core (~200 Fe(III)/shell) that formed endogenously during ferritin expression in *E. coli* has any effect on the protein stability, we compared the thermal denaturation profiles of a *true* apo-ferritin sample expressed in M9 minimal medium (without iron) to that expressed in LB nutritionally rich medium (with iron). Figure 7 revealed insignificant differences between the 2 samples, suggesting that a sizable iron core of several hundred iron atoms is required to significantly alter the protein structure.

2.4.4 | Effect of the iron core size

To test whether the size of the iron core has a cumulative effect on the stability of holo-ferritins, we tested the thermostability of ferritin samples at higher iron loads (i.e., ~1200 Fe(III)/shell total). As seen in Figure 8a, a further decrease in protein stability (5 to 10°C, depending on the protein sample) is observed, indicating a negative correlation between protein stability and the size of the iron core. Interestingly, an indirect relationship between ferritin melting temperature and the size of its iron core is noted in Figure 8b, whereby the larger the size of the iron core, the lower the protein stability.

TABLE 1 Total number of hydrogen bonds and types of H-bonds present in different ferritins from different sources as calculated with HBPLUS (McDonald & Thornton, 1994).

Ferritin source organisms and associated PDB codes	Total H-bonds	MM	SS	MS/SM	Tm (°C)	Ref.
P. furiosus ferritin (2jd6)	4782	3486	776	520	116.8	(Tatur et al., 2007; Yu et al. 2019)
Human L-ferritin (2ffx)	5208	3360	888	960	115	This work
P. yayanosii CH1 ferritin	-	3277**	-	-	112	(Yu et al. 2019)
M. japonicus ferritin (6a4u)	5873	3124	1524	1225	109	(Tan et al. 2021)
Soybean seed H2-ferritin (6j4j)	4916	3096	852	968	106	(Zhang et al. 2019)
T. maritima ferritin (1vlg)	4767	3267	843	657	95	(Chakraborti et al. 2019; Kumar et al. 2021)
Horse spleen ferritin (2w0o)	4920	3072	888	960	93	(Stefanini et al. 1996)
Human H-ferritin (2fha)	4920	3120	816	984	92	This work
A. fulgidus ferritin (1s3q)	4327	3107	628	523	84	(Pulsipher et al., 2017)

Note: MM represents the number of H-bonds formed between main-chain atoms only, MS/SM the number of H-bonds between main-chain and side-chain atoms, and SS the number of H-bonds between side-chain atoms only (SS). The HBPLUS software includes the salt bridges as a subset of the SS H-bonds.
**Calculated by extrapolation since no structure is available for *P. yayanosii*.

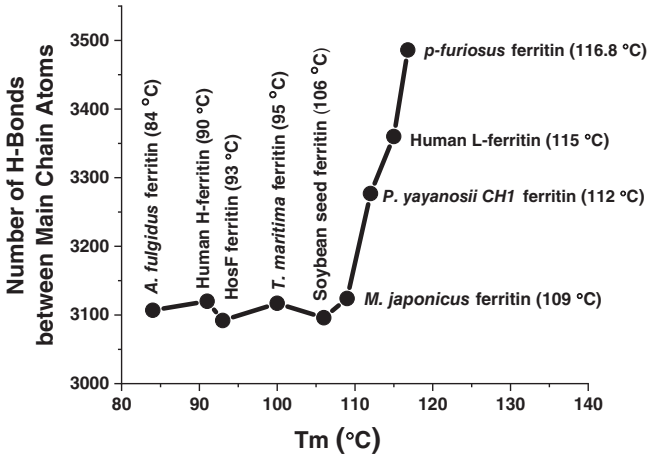

FIGURE 6 Plot of the number of H-bonds present in different types of ferritin versus Tm, according to the data in Table 1. The tertiary and quaternary structure of *P. yayanosii* CH1 ferritin were predicted using the *P. furiosus* ferritin template (PDB ID: 2X17) on the website (https://swissmodel.expasy.org) (Zhang et al., 2019).

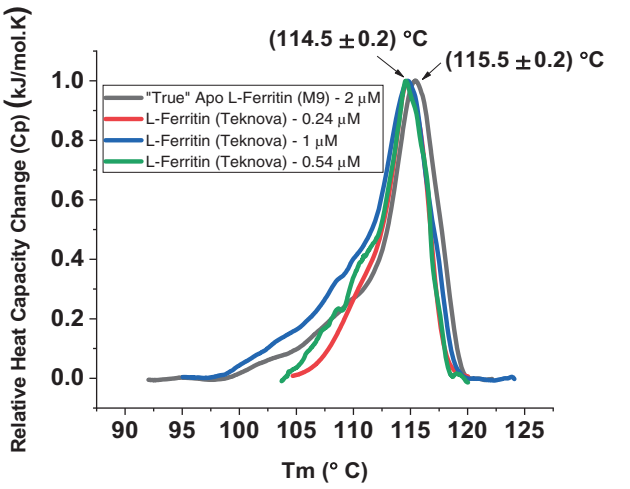

FIGURE 7 Overlay of the relative heat capacity plots versus temperature of iron-free (apo) and iron-containing (~200 Fe(III)/shell) L-homopolymer ferritin samples. Conditions: The concentration of ferritin samples are indicated on the figure and are prepared in 50 mM phosphate buffer, 50 mM NaCl, pH 7.4. The experimental pressure was 3.00 ± 0.03 atm. Note that the L-ferritin samples (H_0:L_{24}) expressed in LB media from Teknova contained ~200 Fe(III)/shell.

2.4.5 | Iron-induced oxidative damage

We then sought to explore whether oxidative damage due to repeated iron injections to the same ferritin sample are the cause of protein damage and thus the observed lower thermal stability. Earlier studies have showed that during Fe(II) oxidation, the ferritin subunits may get damaged and fragmented by hydroxyl radical species generated through Fenton chemistry (Grady et al., 2002), with the H-subunits being more vulnerable than the L-subunits. To test whether any oxidative damage had occurred to our ferritin samples under our experimental conditions, a CGE experiment was performed using homo- and hetero-polymer ferritins, both as apo and holo-proteins. We reasoned that any damage that could have occurred during iron loading would have led to subunits with nicks in their amino acids sequences and would be observed as lower apparent molecular weights on the electropherogram. As seen in Figure 9, the SDS-CGE electropherograms show no difference between the apo and the holo

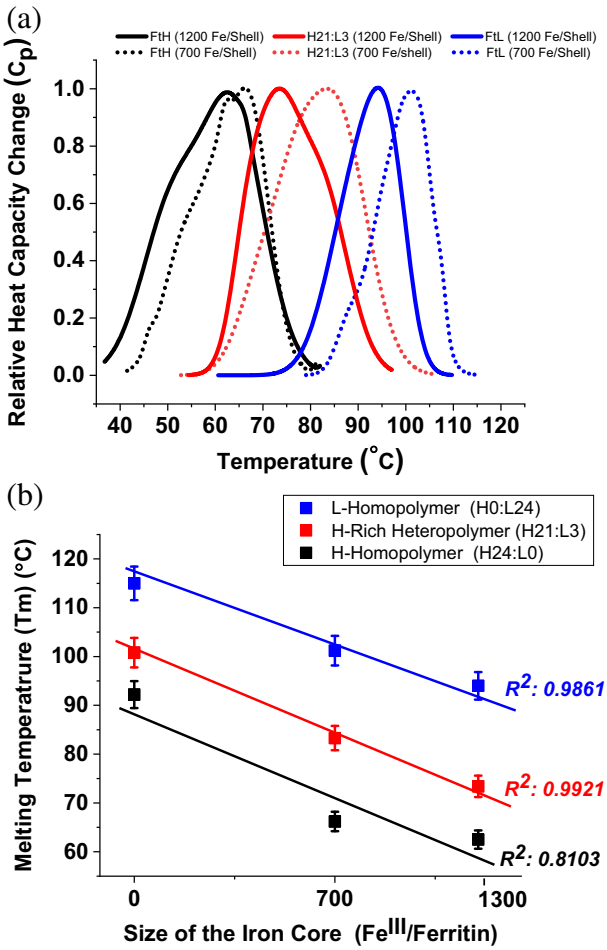

FIGURE 8 (a) Comparison of DSC thermograms (relative heat capacity vs. temperature) of iron-loaded ferritin samples of different core size. Solid lines represent ferritin samples with a core size of ~1200 Fe(III)/shell whereas dotted lines are those containing ~700 Fe(III)/shell. (b) Plot of the melting temperature (Tm) as a function of the size of the ferritin iron core. Conditions: Ferritin samples (0.5 ± 0.1 mg/mL) are prepared in 50 mM phosphate buffer, 50 mM NaCl, pH 7.4. The experimental pressure was 3.00 atm ± 0.03 atm. The error bars represent a standard deviation from multiple runs, at least 2 runs per sample.

samples, suggesting that no damage had occurred to either H or L subunits during iron loading.

3 | DISCUSSION

Using an engineered plasmid in which the H- and L-subunits are controlled by different promoters (IPTG and Tet), various heteropolymer ferritin samples with different H:L subunit ratios have been successfully produced (Srivastava et al., 2021). The observed single bands on native PAGE and the two distinct bands on SDS-PAGE confirmed the formation of heteropolymer ferritin

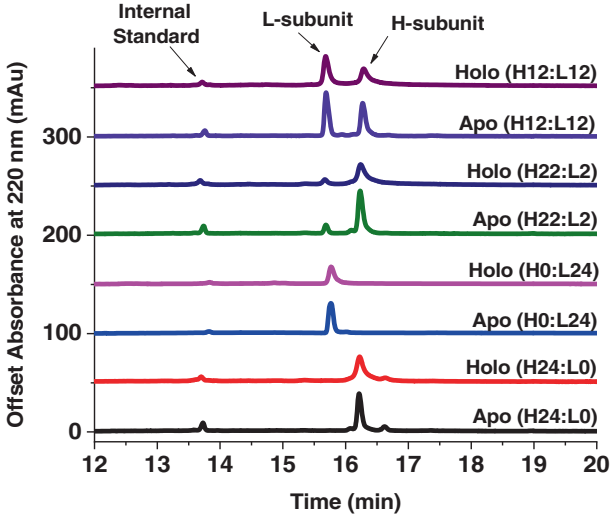

FIGURE 9 SDS-CGE electropherograms of different homo- and heteropolymer ferritin samples prepared in 20 mM MOPS, pH 7.4. The protein concentration was 0.5–0.7 mg/mL; the holo-proteins were loaded with 500 Fe(III)/shell, added in 5 successive injections of 100 Fe(II)/shell, spaced 20–30 min for H_0:L_{24}, 10–15 min for the H_{12}:L_{12}, and 5–10 min for H_{24}:L_0. Note that the absorbance values on the *Y*-axis are arbitrary and have been shifted upward for each of the traces shown above the original black thermogram for easy viewing and comparison.

(Figure 1a,b), the purity and subunits quantification of which were confirmed on CE (Figure 2).

3.1 | Overall ferritin thermal stability

Ferritin thermal stability measurements revealed a complex thermal denaturation profiles involving multiple transitions, for all ferritin samples tested. Due to the complex structure of the 24-mer ferritin and the presence of an extensive and cooperative network of inter- and intra-subunit interactions, we attribute these multi unfolding events to the thermal unfolding of different protein domains (Martsev et al., 1998; Santambrogio et al., 1997; Tatur et al., 2007). Our data do not preclude the possibility that these multi-transitions are due to ferritin shell heterogeneity, or the existence of multiple arrangements of H and L-subunits around the ferritin shell. Purified ferritin sample fractionation using size exclusion chromatography followed by SDS-CGE analysis of the various fractions showed >90% sample homogeneity in terms of subunits composition, suggesting that the observed multi-transitions are unlikely due to ferritin shell heterogeneity. L-homopolymers and L-rich heteropolymers displayed a very high melting temperatures (~115°C) compared to H-homopolymers and H-rich heteropolymers (~90–95°C). This large difference in Tm values is

due to the presence of salt bridges on the L-subunits including a buried salt bridge within the 4-helix bundle, formed between Lys62 and Glu107 which are absent on the H-subunits. The stability of homopolymer H-ferritin is mostly due to a large number of hydrogen bonds, while the homopolymer L-ferritin has more salt bridges on the outside of the subunits, leading to a much higher thermal stability for L-homopolymer and L-rich heteropolymer ferritins (Martsev et al., 1998; Santambrogio et al., 1992). These observations are consistent with electrostatic interactions being one of the major players in protein stability. A closer look at the different classes of H-bonds that keep the ferritin structure together revealed the number of H-bonds formed between main-chain atoms only (MM) plays a critical role in the extra thermostability of human L-ferritin and *P. furiosus* ferritin (Table 1, Figure 6).

Our results agree with a recent study showing that salt bridges formed between Asp132 and Lys128 within the 3-fold channels of prawn ferritin contributed to its higher thermostability (Tm ~109°C), and that mutations of these salt bridges resulted in a strong thermal destabilization (Tm ~91°C) (Tan et al., 2021). Mutations of 3-fold channel residues in homopolymer H-ferritin (E134 to K134) enhanced the protein thermal stability by about 5°C, consistent with a role of salt bridges in stabilizing the ferritin structure (Tan et al., 2021). Other studies have observed an enhancement in the thermal stability of homopolymer H-ferritin following the grafting of a small peptide (30 amino acids) on its N-terminal domain (i.e. Tm ~103°C, a ~20°C improvement over that of H-ferritin alone), and was attributed to new peptide-subunits interactions (Zhang et al., 2019) (i.e., noncovalent, hydrogen bonds, and/or electrostatic interactions). Predictably, the deletion of several N-terminal residues in homopolymer H-ferritin, which are part of a network of interactions at subunit interfaces near the 3-fold channels resulted in a significant reduction in protein stability (Santambrogio et al., 1997).

3.2 | Effect of iron loading on ferritin's structure and stability

Because very little is known about the interactions between ferritin and the iron oxide inside its cavity, it is not clear whether structural changes occur during iron loading into ferritin, and to what extent the integrity of the protein shell is altered by the oxidation of ferrous ions and/or presence of an iron oxide core. Compared to apo-ferritins, our CD results demonstrate a lower helical content, partial unfolding, and a lower thermal stability for the holo-ferritins (Figure 5). These results agree with DSC data which show a difference of 10 to 20°C in Tm values between apo- and holo-ferritins that have at least 700 Fe(III) ions (Figure 4b), and that a larger ferritin iron core of ~1500 Fe(III) ions led to even lower thermostability (Figure 8). Additionally, the DSC measurements revealed an irreversible denaturation process following the first heating step and an inability of the unfolded ferritin to re-fold back to the full 24-mer structure upon cooling, or after sitting for a few hours at room temperature (Figure 4a, inset).

One stimulating possibility for the lower thermal stability of holo-ferritin is that the iron nanoparticles inside the protein could accelerate/facilitate heat transfer from the iron core to the protein moiety leading to protein structural changes or protein damage. Additionally, the observed thermal stability difference between H and L ferritins may be due to different iron core structures or morphologies (Reutovich et al., 2022) with different heat capacities. Although earlier studies have showed that ferritin iron core can be heated by physical stimulations such as microwaves or magnetic fields, a recent study (Meister, 2016) debunked the idea that ferritin iron cores can be heated by magnetic fields. Both theoretical and experimental approaches show that the efficiency of heating magnetic nanoparticles depends strongly on the particle size which plummets steeply below 10 nm (Fortin et al., 2007; Purushotham & Ramanujan, 2010). Magnetite particles smaller than 8 nm are not considered useful for magnetic hyperthermia (Fantechi et al., 2015). Because the size of the ferritin iron core is less than 5 nm in diameter (Longo et al., 2022), and because ferric hydroxide nanomaterial in native ferritin has ~8-fold lower magnetic susceptibility compared to magnetite (Zborowski et al., 1996), the heating rate for ferritin is too low to be measurable and thus could not explain the observed significant drop in stability.

One relevant interpretation for the lower stability of holo-ferritin is that an iron-loaded ferritin could be "sensed" in vivo and primed for degradation and iron recycling. It is possible that endogenous iron loading into ferritin follows an entirely different mechanism than exogenous iron loading, even though the end product is an iron-loaded ferritin (Reutovich et al., 2022). Interestingly, the half-life of ferritin in rat liver was reported to be about 2.5 days (Vulimiri et al., 1977), but in cell culture, the half-life can be as short as 3.5 h (Mehlhase et al., 2005), suggesting that the significant differences between the two environments lead to different processes of ferritin degradation and iron re-cycling. Nonetheless, a less stable holo-ferritin could have important physiological implications since a lower stability for an iron-laden ferritin could facilitate ferritin iron recycling or act as an indicator or sensor for ferritin degradation and iron

retrieval (Santana-Codina & Mancias, 2018; Smith et al., 2022). Significantly, when iron-loaded ferritins (~1500 Fe(III)/shell) were stripped of iron using a reductive iron mobilization process (Bou-Abdallah et al., 2018), the resulting apo-ferritins did not regain their higher stability, compared to holo-ferritins, and showed signs of precipitation, suggesting an irreversible unfolding/destabilization process, at least under our DSC experimental conditions (3 atm and 25–130°C, Figure 1S). While human H-homopolymer ferritin (H_{24}:L_0) regained some of its original stability following iron removal (Figure 1S, blue curves), heteropolymer H-rich ferritin (H_{21}:L_3) stability did not improve (Figure 1S, red curves), suggesting that the destabilization effect is not a fully reversible process, and that once the complex web of inter-and intra-subunit interactions is disrupted, the protein is unable to reassemble back to its original structure. After the DSC experiments (Figure 1S), native-PAGE of the two ferritin samples (H_{24}:L_0 and H_{21}:L_3) showed faint bands (Lanes 2 and 6, Gel A, and lanes 3 and 7, Gel B, Figure 2S), consistent with a partial protein recovery. These results are supported by additional DSC measurements (Figure 4c) demonstrating that a full recovery or refolding of ferritin samples upon cooling (or after sitting for a few hours at room T) does not occur.

An earlier study using small-angle x-ray scattering (SAXS) and small-angle neutron scattering (SANS) showed significant structural changes of the protein shell at moderate (~ 800 Fe/shell) iron loading, resulting in structure and size polydispersity (distribution of iron loading between the ferritin molecules), partial ferritin shell damage and ferritin subunit disassembly (Melníková et al., 2014). Our results agree with this early report and, in addition, suggest that the more L-subunits present on the ferritin shell, the less the damage (e.g. the difference in Tm values between apo- and holo-ferritins in the L- and L-rich samples is ~12–14°C compared to ~18–20°C for the H- and H-rich samples, Figure 4b inset), consistent with a more robust L-ferritin structure. Furthermore, it is interesting to consider the 30°C lower melting transitions of ferritin channels variants compared to those at which the ferritin global structure melts. Whereas the ferritin structure is stable up to 6-8 M urea (or GnHCl) at neutral pH (Harrison & Arosio, 1996) and temperatures of ~90°C (Crichton & Declercq, 2010) or even more (i.e. up to 115°C, depending on the ferritin type - this work), it has been shown that a 10°C downshift in melting transition occurs in the presence of low chaotrope concentrations (0.01–1 M urea or guanidine), indicating high sensitivity of ferritin pores (or channels) to small changes in heat or physiological urea concentration (Hasan et al., 2008; Liu et al., 2003; Theil et al., 2008). Similar changes were noted when amino acid substitutions in or around the 3-fold channels were made by site-directed mutagenesis. We speculate that iron loading may also destabilize local structures around 3-fold channels leading to lower overall stability of the globular ferritin structure. Such structural modifications would suggest the presence of biomolecules or biological regulators in cells that could recognize these changes and either (1) make the ferritin iron mineral accessible to cellular reductants to maintain cellular iron homeostasis, (2) bring the ferritin molecule to the lysosome for proteolysis and iron release (Santana-Codina & Mancias, 2018; Smith et al., 2022), or (3) sequester ferritin as lysosomal hemosiderin when there is excess iron and no cellular need for it. Altogether, our data indicate that structural changes occur during exogenous iron loading into ferritin, but that the integrity of the protein shell is not altered by the oxidation of ferrous ions and/or the presence of an iron oxide core.

In summary, the high intrinsic thermal stability of recombinant human ferritin (both homopolymer H- and L-ferritins and heteropolymer ferritins of different H to L subunit ratios) is likely due to the presence of an extensive co-operative network of inter- and intra-subunit interactions (i.e., hydrophobic, electrostatic, hydrogen bonds, and salt bridges) but also to secondary structural composition. The hyperthermostability of homopolymer L- and L-rich ferritins (Tm of 115°C) demonstrate a critical role for the L-subunits in the overall thermal stability of these proteins. Although recent studies have shown that some animal and plant ferritins (Tan et al., 2021; Zhang et al., 2019) can display high thermostability (e.g., prawn ferritin, Tm 109°C, and soybean seed ferritin, Tm 106°C), our study demonstrates that the Tm values of recombinant L and L-rich human ferritins are very close to or even surpass many known hyperthermostable ferritins including those from thermophilic organisms such as archaea and bacteria (Szilagyi & Zavodszky, 2000; Tatur et al., 2007; Vieille & Zeikus, 2001). This extraordinary stability may facilitate the use of human ferritin in a variety of applications, from a robust bio/nano template for the design of bio/nano materials (Fan et al., 2012; Mohanty et al., 2022), to the encapsulation and delivery of bioactive compounds and drugs (Cai et al., 2019; Chiou & Connor, 2018; Truffi et al., 2016), and in industrial food science applications particularly those that require thermal processing (Xing et al., 2022; Zhang et al., 2017).

4 | MATERIALS AND METHODS

4.1 | Ferritin expression and purification

Recombinant human homopolymer and heteropolymer ferritins with different H to L subunit ratios were

produced in *Escherichia coli* Rosetta-gami B strain using a recently engineered pWUR-FtH-TetO-FtL plasmid and different concentrations of inducers, as described in detail elsewhere (Srivastava et al., 2021). Protein purification and quantification were performed according to established protocols using size exclusion chromatography (Akta Go, GE Healthcare), native and SDS-PAGE, and CGE (7100 model from Agilent Technologies) (Srivastava et al., 2021). Protein concentrations were determined using the Micro BCA (bicinchoninic acid) Protein Assay Kit and a Varioskan LUX microplate reader from Thermo Fisher Scientific. Purified recombinant homopolymer and heteropolymer ferritins contained a small iron core (i.e., $< 200 \pm 50$ Fe(III)/ferritin molecule), as determined by an iron reductive mobilization assay (Bou-Abdallah et al., 2018). Therefore, to preserve the integrity of the ferritin shell and avoid oxidative damage due to harsh chemical treatments, we opted to use all purified ferritin samples in this study as expressed in *E. coli*, and without the removal of this small iron core. In this study, we refer to these ferritin samples as apo-ferritin, and the exogenously iron-loaded samples as holo-ferritin.

4.2 | Chemicals and reagents

Dibasic anhydrous sodium phosphate and ferrous sulfate heptahydrate ($FeSO_4{\cdot}7H_2O$) were purchased from Fisher Scientific, MOPS (3-[N-morpholino]propanesulfonic acid) and sodium chloride from Sigma-Aldrich.

4.3 | Iron loading into ferritin

Iron solutions were prepared by dissolving ferrous iron sulfate in deionized water adjusted to pH 2.0 with hydrochloric acid, and then filtered through 0.2 μm Whatman Puradisc polyethersulfone sterile syringe filters from Cytiva. Typically, 5 μl injections of a stock ferrous sulfate solution was added to a 1 ml protein solution prepared in 20 mM Mops, pH 7.4 sitting in a quartz cuvette to achieve a desired iron/protein ratio (e.g., 100 Fe(II)/shell per injection, or 5 injections for a total of 500 Fe/shell). The Fe(II) oxidation kinetics were followed under constant stirring on a Varian Cary 50 Bio or Cary 60 spectrophotometers from Agilent Technologies at 305 nm where the Fe(III) oxo(hydroxo) species absorbs (Mehlenbacher et al., 2017). The iron-loaded ferritin samples (holo-ferritin) were centrifuged and then extensively dialyzed against 50 mM phosphate, 50 mM NaCl buffer, pH 7.4. Because H- and H-rich ferritins oxidize ferrous ions much faster than L and L-rich ferritins, adequate time (~ 10 min for H- and H-rich ferritins, and ~20 min for L- and L-rich ferritins) was allowed for each injection of 100 Fe(II)/shell (Mehlenbacher et al., 2017; Srivastava et al., 2021).

4.4 | Capillary gel electrophoresis (SDS-CGE)

To quantify the integrity and the H- and L-subunit composition of purified recombinant human homopolymer and heteropolymer ferritins, CGE was used under denaturing conditions (SDS-CGE). The reagents of the Sciex CE-SDS analysis kit include SDS-MW gel buffer (proprietary formulation, pH 8, 0.2% SDS), CE SDS sample buffer (100 mM Tris–HCl pH 9.0, 1% SDS), acidic wash solution (0.1 N HCl), and basic wash solution (0.1 N NaOH). An Agilent Technologies 50 μm ID bare fused silica capillary, with a total length of 33 cm and an effective length 24.5 cm was used in the SDS-CGE experiments. The SDS-CGE capillary was pre-conditioned under a high pressure of 2.0 bar using 0.1 N NaOH (10 min), 0.1 N HCl (5 min), water (2 min), and finally a high-pressure flush (4.0 bar) of the SDS gel buffer for 10 min. Prior to each protein run, the capillary was conditioned under a high-pressure flush of 4 bar using 0.1 N NaOH (3 min), 0.1 N HCl (1 min), water (1 min) and finally SDS gel buffer (10 min). The protein samples were injected electrokinetically by applying a negative voltage of - 5 kV for 20 s. Protein subunits separation was followed under a negative applied voltage of - 16.5 kV for 30 min. A 2.0 bar pressure was applied to both inlet and outlet vials for the duration of the experiment with the capillary temperature maintained at 25.00°C. The detection wavelength was set at 220 nm (10 nm bandwidth) with a 350 nm reference wavelength (10 nm bandwidth) and a response time of 1 s. Typically, ferritin solutions (100 ml at 1–2 mg/mL) were prepared in an SDS sample buffer (>60% by volume) in the presence of 5 μl 2-beta-mercaptoethanol (5% v/v) from Sigma-Aldrich. The ferritin solution was mixed thoroughly, tightly capped and heated in a 100°C water bath for 5–10 min. The protein solution was then cooled to room temperature prior to running on the 7100-model capillary electrophoresis instrument from Agilent Technologies.

4.5 | Differential scanning calorimetry (DSC)

DSC experiments were performed on a NanoDSC instrument from TA Instruments under a constant pressure of 3 atm, in the temperature range of 25–125°C, using a

scan rate of 1°C/min. All ferritin samples (0.5 ± 0.1 mg/mL) were dialyzed several times in 50 mM phosphate buffer, 50 mM NaCl, pH 7.4 and degassed for 20 minutes prior to analysis using the TA Instruments degassing station. DSC experiments were performed 2 to 3 times to ensure reproducibility. The DSC raw thermograms (μW) were converted to molar heat capacity (kJ/mol.K), corrected by subtracting a buffer–buffer background scan, and then analyzed using the TA Instruments DSC NanoAnalyze software. Unfortunately, due to the complex nature of the ferritin unfolding processes and domain cooperativity (i.e., broad and multiple transitions), our attempts to deconvolute the multi-transition unfolding events using multiple Gaussian models paired with a polynomial baseline analysis were unsuccessful and provided insignificant and unreliable results. Nonetheless, Tm values (i.e., melting temperatures at which 50% of the molecules are unfolded and determined from the maximum heat capacity melting curves) were quite reliable and reproducible between different sample preparations and experiments. After the first heating step, the ferritin samples were fully unfolded and did not refold back to their original structures upon cooling, or after sitting for a few hours at room temperature. A second heating step shows no observable signal suggesting that all DSC measurements represent irreversible denaturation of ferritin, with empirical Tm values, and not an equilibrium between the folded and unfolded states.

4.6 | Circular dichroism (CD)

The secondary structures of two heteropolymer H_{19}:L_5 ferritin samples, an iron-free sample and an iron-loaded sample at ~1000 Fe/shell, both at 0.2 mg/mL, were obtained on an Aviv model 420 spectrometer equipped with thermoelectric heating/cooling. The two samples were initially prepared in 50 mM Mops, 100 mM NaCl, pH 7.5. After iron loading, both samples were dialyzed against water pH 7.5 and the CD spectra were recorded between 250 and 200 nm using 1 mm path length cuvette. Thermal melts were recorded in 2°C increments over the temperature range of 20–90°C with a heating rate of 10°C/min.

AUTHOR CONTRIBUTIONS

Ayush K. Srivastava: Conceptualization (equal); formal analysis (equal); investigation (equal); methodology (equal). **Lucas J. Scalcione:** Formal analysis (equal); investigation (equal); methodology (equal). **Paolo Arosio:** Formal analysis (equal); investigation (equal); methodology (equal); writing – review and editing (equal). **Fadi Bou-Abdallah:** Conceptualization (equal); data curation (equal); formal analysis (equal); funding acquisition (equal); investigation (equal); methodology (equal); project administration (equal); supervision (equal); writing – original draft (equal); writing – review and editing (equal).

ACKNOWLEDGMENTS

This work is supported by the National Science Foundation, Division of Molecular and Cellular Biosciences (MCB) award 1934666 (F.B.-A.), an NSF Major Research Instrumentation Program (NSF MRI Award 0921364) (F.B.-A), the National Institute of Health grant R15GM104879 (F.B.-A.), and a Cottrell Instrumentation Supplements Award from the Research Corporation for Science Advancement award #27452 (F.B.-A.).

ORCID

Fadi Bou-Abdallah https://orcid.org/0000-0002-8557-1827

REFERENCES

Arosio P, Ingrassia R, Cavadini P. Ferritins: a family of molecules for iron storage, antioxidation and more. Biochim Biophys Acta Gen Subj. 2009;1790:589–99.

Bou-Abdallah F. The iron redox and hydrolysis chemistry of the ferritins. Biochim Biophys Acta Gen Subj. 2010;1800:719–31.

Bou-Abdallah F, Paliakkara JJ, Melman G, Melman A. Reductive mobilization of iron from intact ferritin: mechanisms and physiological implication. Pharmaceuticals. 2018;11(4):120.

Cai Y, Wang Y, Xu H, Cao C, Zhu R, Tang X, et al. Positive magnetic resonance angiography using ultrafine ferritin-based iron oxide nanoparticles. Nanoscale. 2019;11:2644–54.

Carmona F, Poli M, Bertuzzi M, Gianoncelli A, Gangemi F, Arosio P. Study of ferritin self-assembly and heteropolymer formation by the use of fluorescence resonance energy transfer (FRET) technology. Biochim Biophys Acta Gen Subj. 2017;1861:522–32.

Chakraborti S, Korpi A, Kumar M, Stępień P, Kostiainen MA, Heddle JG. Three-dimensional protein cage Array capable of active enzyme capture and artificial chaperone activity. Nano Lett. 2019;19:3918–24.

Chasteen ND, Harrison PM. Mineralization in ferritin: an efficient means of iron storage. J Struct Biol. 1999;126:182–94.

Chiou B, Connor JR. Emerging and dynamic biomedical uses of ferritin. Pharmaceuticals. 2018;11:124.

Cozzi A, Corsi B, Levi S, Santambrogio P, Albertini A, Arosio P. Overexpression of wild type and mutated human ferritin H-chain in HeLa cells in vivo role of ferritin ferroxidase activity. J Biol Chem. 2000;275:25122–9.

Crichton RR, Declercq JP. X-ray structures of ferritins and related proteins. Biochim Biophys Acta. 2010;1800:706–18.

Fan k, Cao C, Pan Y, Lu D, Yang D, Feng J, et al. Magnetoferritin nanoparticles for targeting and visualizing tumour tissues. Nat Nanotechnol. 2012;7:459–64.

Fantechi E, Innocenti C, Albino M, Lottini E, Sangregorio C. Influence of cobalt doping on the hyperthermic efficiency of magnetite nanoparticles. J Magn Magn Mat. 2015;380:365–71.

Fortin JP, Wilhelm C, Servais J, Menager C, Bacri JC, Gazeau F. Size-sorted anionic iron oxide nanomagnets as colloidal

mediators for magnetic hyperthermia. J Am Chem Soc. 2007; 129:2628–35.
Grady JK, Zang J, Laue TM, Arosio P, Dennis CN. Characterization of the H- and L-subunit ratios of ferritins by sodium dodecyl sulfate–capillary gel electrophoresis. Anal Biochem. 2002;302: 263–8.
Hamburger AE, West AP Jr, Hamburger ZA, Hamburger P, Bjorkman PJ. Crystal structure of a secreted insect ferritin reveals a symmetrical arrangement of heavy and light chains. J Mol Biol. 2005;349:558–69.
Harrison PM, Arosio P. The ferritins: molecular properties, iron storage function and cellular regulation. Biochim Biophys Acta—Bioenerg. 1996;1275:161–203.
Hasan MR, Tosha T, Theil EC. Ferritin contains less iron (59Fe) in cells when the protein pores are unfolded by mutation. J Biol Chem. 2008;283(46):31394–400.
Kumar M, Markiewicz-Mizera J, David Janna Olmos J, Wilk P, Grudnik P, Biela AP, et al. A single residue can modulate nanocage assembly in salt dependent ferritin. Nanoscale. 2021; 13:11932–42.
Lawson DM, Treffry A, Artymiuk PJ, Harrison PM, Yedall SJ, Luzzago A, et al. Identification of the ferroxidase Centre in ferritin. FEBS Lett. 1989;254:207–10.
Levi S, Santambrogio P, Albertini A, Arosio P. Human ferritin H-chains can be obtained in non-assembled stable forms which have ferroxidase activity. FEBS Lett. 1993;336:309–12.
Levi S, Santambrogio P, Cozzi A, Rovida E, Corsi B, Tamborini E, et al. The role of the L-chain in ferritin iron incorporation. Studies of homo and Heteropolymers. J Mol Biol. 1994;238(5):649–54.
Liu X, Jin W, Theil EC. Opening protein pores with chaotropes enhances Fe reduction and chelation of Fe from the ferritin biomineral. Proc Natl Acad Sci. 2003;100(7):3653–8.
Longo T, Kim S, Srivastava AK, Hurley L, Ji K, Viescas AJ, et al. Micromagnetic and morphological characterization of heteropolymer human ferritin cores. Nanoscale Adv. 2023;5:208–19.
Lopez-Castro JD, Delgado JJ, Perez-Omil JA, Galvez N, Cuesta R, Watt RK, et al. A new approach to the ferritin iron core growth: influence of the H/L ratio on the core shape. Dalton Trans. 2012;41:1320–4.
Martsev SP, Vlasov AP, Arosio P. Distinct stability of recombinant L and H subunits of human ferritin: calorimetric and ANS binding studies. Protein Eng. 1998;11(5):377–81.
McDonald IK, Thornton JM. Satisfying hydrogen bonding potential in proteins. J Mol Biol. 1994;238(5):777–93.
McNally JR, Mehlenbacher MR, Luscieti S, Smith GL, Reutovich AA, Maura P, et al. Mutant L-chain ferritins that cause neuroferritinopathy alter ferritin functionality and iron permeability. Metallomics. 2019;11(10):1635–47.
Mehlenbacher M, Poli M, Arosio P, Santambrogio P, Levi S, Chasteen ND, et al. Iron oxidation and core formation in recombinant heteropolymeric human ferritins. Biochemistry. 2017;56:3900–12.
Mehlhase J, Sandig G, Pantopoulos K, Grune T. Oxidation-induced ferritin turnover in microglial cells: role of proteasome. Free Radic Biol Med. 2005;38:276–85.
Meister M. Physical limits to magnetogenetics. eLife. 2016;5:e17210.
Melníková L, Petrenko VI, Avdeev MV, Garamus VM, Almásy L, Ivankov OI, et al. Effect of iron oxide loading on magnetoferritin structure in solution as revealed by SAXS and SANS. Colloids Surf B Biointerfaces. 2014;123(1):82–8.
Mohanty A, Parida A, Raut RK, Behera RK. Ferritin: a promising Nanoreactor and Nanocarrier for bionanotechnology. ACS Bio Med Chem Au. 2022;2:258–81.
Pozzi C, Ciambellotti S, Bernacchioni C, Di Pisa F, Mangani S, Turano P. Chemistry at the protein–mineral interface in L-ferritin assists the assembly of a functional (μ3-oxo)Tris [(μ2-peroxo)] tri-iron(III) cluster. Proc Natl Acad Sci. 2017;114: 2580–5.
Pulsipher KW, Villegas JA, Roose BW, Hicks TL, Yoon J, Saven JG, et al. Thermophilic ferritin 24mer assembly and nanoparticle encapsulation modulated by Interdimer electrostatic repulsion. Biochemistry. 2017;56(28):3596–606.
Purushotham S, Ramanujan RV. Modeling the performance of magnetic nanoparticles in multimodal cancer therapy. J Appl Phys. 2010;107:114701.
Reutovich AA, Srivastava AK, Smith GL, Foucher A, Yates DM, Stach EA, et al. Effect of phosphate and ferritin subunit composition on the kinetics, structure, and reactivity of the iron Core in human homo and Heteropolymer ferritins. Biochemistry. 2022;61(19):2106–17.
Santambrogio P, Levi S, Arosio P, Palagi L, Vecchio G, Lawson D, et al. Evidence that a salt bridge in the light chain contributes to the physical stability difference between heavy and light human ferritins. J Biol Chem. 1992;267:14077–83.
Santambrogio P, Levi S, Cozzi A, Rovida E, Albertini A, Arosio P. Production and characterization of recombinant Heteropolymers of human ferritin H and L chains. J Biol Chem. 1993; 268(17):12744–8.
Santambrogio P, Pinto P, Levi S, Cozzi A, Rovida E, Artymiuk P, et al. Effects of modifications near the 2-, 3- and 4-fold symmetry axes on human ferritin renaturation. Biochem J. 1997;322: 461–8.
Santana-Codina N, Mancias JD. The role of NCOA4-mediated ferritinophagy in health and disease. Pharmaceuticals. 2018;11:114.
Simonetta Stefanini S, Cavallo S, Wang CQ, Tataseo P, Vecchini P, Giartosio A, et al. Thermal stability of horse spleen Apoferritin and human recombinant H Apoferritin. Arch Biochem Biophys. 1996;325(1):58–64.
Smith GL, Srivastava AK, Reutovich AA, Hunter NJ, Arosio P, Melman A, et al. Iron mobilization from ferritin in yeast cell lysate and physiological implications. Int J Mol Sci. 2022;23: 6100.
Srivastava A, Arosio P, Poli M, Bou-Abdallah F. A novel approach for the synthesis of human Heteropolymer ferritins of different H to L subunit ratios. J Mol Biol. 2021;433(19):167198.
Szilagyi A, Zavodszky P. Structural differences between mesophilic, moderately thermophilic and extremely thermophilic protein subunits: results of a comprehensive survey. Structure. 2000;8: 493–504.
Tan X, Liu Y, Zang J, Zhang T, Zhao G. Hyperthermostability of prawn ferritin nanocage facilitates its application as a robust nanovehicle for nutraceuticals. Int J Biol Macromol. 2021;191: 152–60.
Tatur J, Hagen WR, Matias PM. Crystal structure of the ferritin from the hyperthermophilic archaeal anaerobe *Pyrococcus furiosus*. J Biol Inorg Chem. 2007;12:615–30.
Theil EC. Ferritin: the protein nanocage and iron biomineral in health and in disease. Inorg Chem. 2013;52:12223–33.
Theil EC, Liu XS, Tosha T. Gated pores in the ferritin protein nanocage. Inorg Chim Acta. 2008;361:868–74.

Theil EC, Tosha T, Behera RK. Solving biology's iron chemistry problem with ferritin protein nanocages. Acc Chem Res. 2016; 49:784–91.

Truffi M, Fiandra L, Sorrentino L, Monieri M, Corsi F, Mazzucchelli S. Ferritin nanocages: a biological platform for drug delivery, imaging and theranostics in cancer. Pharmacol Res. 2016;107:57–65.

Vieille C, Zeikus GJ. Hyperthermophilic enzymes: sources, uses, and molecular mechanisms for Thermostability. Microbiol Mol Biol Rev. 2001;65(1):1–43.

Vulimiri L, Linder MC, Munro HN. Sex difference in the distribution and iron responsiveness of rat cardiac and skeletal muscle ferritins. Biochim Biophys Acta. 1977;497:280–7.

Xing Y, Ma J, Yao Q, Chen X, Zang J, Zhao G. The change in the structure and functionality of ferritin during the production of pea seed Milk. Foods. 2022;11:557.

Yu J, Zhang T, Xu H, Dong X, Cai Y, Pan Y, et al. Thermostable iron oxide nanoparticle synthesis within recombinant ferritins from the hyperthermophile *Pyrococcus yayanosii* CH1. RSC Adv. 2019;9:39381–93.

Zborowski M, Fuh CB, Green R, Baldwin NJ, Reddy S, Douglas T, et al. Immunomagnetic isolation of magnetoferritin-labeled cells in a modified ferrograph. Cytometry. 1996;24:251–9.

Zhang C, Zhang X, Zhao G. Ferritin Nanocage: a versatile Nanocarrier utilized in the field of food, nutrition, and medicine. Nanomaterials. 2020;10:1894.

Zhang S, Zang J, Chen H, Li M, Xu C, Zhao G. The size flexibility of ferritin Nanocage opens a new way to prepare nanomaterials. Small. 2017;1701045.

Zhang X, Zang J, Chen H, Zhou K, Zhang T, Lv C, et al. Thermostability of protein nanocages: the effect of natural extra peptide on the exterior surface. RSC Adv. 2019;9:24777–82.

SUPPORTING INFORMATION

Additional supporting information can be found online in the Supporting Information section at the end of this article.

How to cite this article: Srivastava AK, Scalcione LJ, Arosio P, Bou-Abdallah F. Hyperthermostable recombinant human heteropolymer ferritin derived from a novel plasmid design. Protein Science. 2022. e4543. https://doi.org/10.1002/pro.4543